LA-UR-03-3105

Approved for public release; distribution is unlimited.

Title: Residual stresses in LENS® components using neutron diffraction and contour method

Author(s): P. Rangaswamy (1), M.L. Griffith (2), T, M. Holden (1), M.B. Prime (1), and R. B. Rogge (3)
(1) LANL, Los Alamos, NM 87545, USA
(2) SNL, Albuquerque, NM 87185, USA
(3) National Research Council of Canada, Chalk River, Canada

Submitted to: Materials Science and Engineering A, 399(1-2), pp. 72-83, 2005.

Residual stresses in LENS® components using neutron diffraction and contour method

P. Rangaswamy[1], M.L. Griffith[2], M.B. Prime[1], T, M. Holden[1], R. B. Rogge[3], J. M. Edwards[1] and R. J. Sebring[1]

[1]Los Alamos National Laboratory, Los Alamos, NM 87545, USA
[2]Sandia National Laboratories, Albuquerque, NM 87185, USA
[3]National Research Council of Canada, Chalk River Laboratories Chalk River, ON K0J 1J0,Canada

Abstract

During manufacturing of components using the Laser Engineered Net Shaping (LENS®), a solid freeform fabrication process the introduction of residual stresses causes problems associated with deformation or in the worst case cracking. The origin is attributed to thermal transients encountered during solidification. In the absence of reliable predictive models for the residual stresses, measurements are imperative. Residual stresses were measured in LENS® samples (316 Stainless Steel and Inconel 718) having simple geometrical shapes by using both neutron diffraction and the contour method, the latter which provides spatial distribution normal to the plane of sectioning. Using the L3 spectrometer at Chalk River Laboratories (Canada), stresses were mapped spatially with sampling volumes ranging from 2 to 10 mm^3 in three orthogonal directions. The neutron and contour method, results are compared and discussed in the context of growth direction during the LENS® process. The residual stresses were surprisingly uni-axial, with high stresses in the growth direction and near-zero stresses transverse. The similarity of the contour method measurements on the two distinct materials indicated that the stresses primarily arose from thermal transients rather than from material-dependent causes like phase transformations. Neutron measurements in the stainless steel specimen using one reflection (the {002}) sensitive to intergranular stress and another (the {113}) sensitive only to macrostresses indicated that the stresses arose from elastic deformation only, without significant plasticity.

Keywords: neutron diffraction, contour method, residual stresses, Laser Engineered Net Shaping (LENS®).

Partha Rangaswamy

partha@lanl.gov (505 667 2935)

Residual stresses in LENS® components using neutron diffraction and contour method

1. Introduction

Laser engineering net shaping is a laser fabrication technique developed at Sandia National Laboratory for producing components that are difficult or impossible to process through conventional metal forming techniques [1-4]. LENS® is a fabrication process that fuses metal powder fed to the focal zone of a laser to produce 3-dimensional metal components. LENS® has many potential applications, including rapid prototyping, rapid tooling, and dissimilar metal joining. Samples have been successfully manufactured from a variety of materials including steels, stainless steels (SS), nickel-based alloys, refractory metals, and intermetallic compounds. Fabrications of bi-material joints as well as functionally graded materials through the use of LENS® have also been successfully processed.

By its nature, LENS® is a near net shaping process, which means that the components would generally require finish machining. Experience has shown that this finish machining is greatly complicated by residual stresses locked into the parts during the building process. LENS® employs a laser focused onto a metal substrate positioned on two axes. The focused laser creates a small weld pool into which powdered metal is deposited. By rastering the part under the focal point, line-by-line and layer-by-layer, a part is built up in a method similar to conventional rapid prototyping. Because of this layer additive process, the localized heat of the melt pool passes over a point, and then next to the point as successive hatch lines are deposited. Then this point experiences localized heating again and again as each layer is deposited. This cyclic heating and cooling locks stress into the component in a manner that is very difficult to model analytically despite some ongoing efforts [5,6]. When the component is finish machined, the stress is relieved causing part movement that greatly complicates the machining process.

It is imperative that an understanding of the residual stress in the components be found. This understanding will help in research aimed at reducing the stresses either fabrication or in subsequent heat treatment. An understanding of the stresses will also aid in planning the machining process for these components. Residual stresses have previously been determined on the surface of LENS® parts by hole drilling combined with laser holography [7,8]. The measurements revealed stresses at some locations with magnitudes that were about 75% of the yield strength of the material. However, the holographic hole drilling only measured to a depth of 0.75mm, and it is critical to know the stress state throughout the material. The hole drilling measurements also had problems because the high stress magnitudes sometimes caused yielding during the measurement, invalidating the results.

On the other hand, neutrons penetrate easily into most materials and neutron diffraction is a well-established method for non-destructively mapping residual stresses inside metallic engineering components. The residual stress distributions in two Laser Engineered Net Shaping (LENS®) 316 stainless steel samples were mapped previously by neutron diffraction [8]. The samples took the form of a thin wall and a pillar of square cross section. Stresses were measured in the three orthogonal symmetry directions of the parts, parallel and perpendicular to the growth direction. Surprisingly, over most of

the bulk of the samples the stress was uniaxial and directed along the growth axis with compression in the center of the samples and tension at the edges. The magnitudes of the maximum residual stresses were significant fractions (50% and 80% for the thin wall and pillar respectively) of the 0.2% yield point of ~450 MPa [1].
In the absence of model predictions (analytical or numerical), which could be validated by experiment results, further measurements become necessary to understand whether the effects of laser rastering directions (per layer) have any influence on residual stresses. Furthermore, the question whether the deformation as a result of inhomogeneous temperature distribution throughout the component would be solely elastic or include both elastic and plastic effects can also be examined using neutron diffraction. In addition the availability of a relatively new but powerful technique such as contour method [9] would allow us to verify the residual stresses determined using both neutron diffraction and holographic techniques. The spatial resolution of the contour method provides a detailed 2-D map of the normal stress component to the plane of a cut. The contour method has been experimentally validated by comparing with neutron diffraction measurements on a weldment [10], and has often been applied to specimens whose large cross-sectional areas limits the applicability of neutron diffraction due to limited penetration [11,12]. Since the maximum residual stresses are primarily oriented along the growth direction for LENS® samples, the direct comparison with contour method will not only provide answers for components whose cross-sectional areas limits the applicability of neutron diffraction but also for materials where the presence of multiple phases, absence of crystallinity, texture or preferred orientation (e.g. single crystals) and grain sizes would render the measurements in-applicable or generate sources of errors which are extremely difficult to account for.

In this paper we present the results from several residual stress measurements on LENS® samples of different materials and sizes. Neutron diffraction was applied to LENS® samples of 316 stainless steel to study the effects of laser rastering, effects of plasticity on residual stresses. The contour method was applied to both 316 stainless steel and Inconel 718 samples of square cross-sections. The laser rastering studies were performed using neutron diffraction on three 316 stainless steel samples with rectangular cross-section. The effect of elastic or elastic and plastic effects on residual stresses were examined on the 316 stainless steel pillar sample of the same material also with neutron diffraction. The contour method was applied to pillar samples of both 316 stainless steel and Inconel 718.

2. Theory

2.1. Neutron Diffraction

2.1.1 Definition of Strain and Stress

The neutron diffraction technique for making strain measurements makes use of Bragg's law [13],

$$\lambda = 2d_{hkl}\sin\theta_{hkl} \qquad (1)$$

to relate the neutron wavelength, λ, the measured angle of diffraction, $2\theta_{hkl}$, and the lattice spacing, d_{hkl}, of the lattice planes identified by Miller indices (hkl). The elastic lattice strain at a particular location is derived from the change of the experimental lattice spacing with respect to an appropriate stress-free reference lattice spacing, d^0_{hkl}, as follows

$$\varepsilon_{hkl} = \frac{d_{hkl} - d^0_{hkl}}{d^0_{hkl}} \qquad (2)$$

Three orthogonal elastic stress components (e.g. σ_x, σ_y, and σ_z), directed along the geometrical axes (X, Y, Z) shown in Figure 1, may be calculated from three measured components of elastic strain (ε_X, ε_Y, ε_Z) with Hooke's Law, which is written for the component σ_x as,

$$\sigma_X = \frac{E_{hkl}((1-\nu_{hkl})\varepsilon_X + \nu_{hkl}\varepsilon_Y + \nu_{hkl}\varepsilon_Z)}{(1+\nu_{hkl})(1-2\nu_{hkl})} \qquad (3)$$

Here, E_{hkl} is the diffraction elastic constant analogous to Young's modulus and ν_{hkl} is analogous to Poisson's ratio. Diffraction elastic constants relate the elastic lattice strain in the direction normal to the {hkl} plane used in the diffraction measurement, to the macroscopic stress field. The diffraction elastic constants for the {113} reflection, used for the measurements were calculated from the Kröner [14] model using the measured single crystal elastic constants [15], and, are E_{113}=184 GPa and ν_{113}=0.294. The calculated bulk elastic constant E_{bulk}=196 GPa is in good agreement with other accepted values of the bulk elastic constant, 193 GPa for 316 stainless steel [16].

2.1.2 Plasticity effects on diffraction strain and stress measurements

It has been shown [17,18] for stainless steel that the {113} reflection has a small contribution from intergranular effects and may be taken to give a correct measure of the strains corresponding to the macroscopic stress field. For this reason the {113} reflection was chosen to map the stress field in the present experiments.

Residual stresses originate in the inhomogeneous deformation of components and materials. In the present case it is likely that an inhomogeneous temperature distribution throughout the component, i.e. a thermal gradient, generates the stresses. The deformation resulting from the temperature differences may be solely elastic or may involve both elastic and plastic effects. The residual stresses are on two length scales: the length scale imposed by the dimensions of the work-piece, which corresponds to the macroscopic stress field, and the length scale of the grains making up the work-piece, which corresponds to intergranular or type-2 stresses. Intergranular stresses arise because of the anisotropy of the elastic properties and the slip processes with respect to the crystallographic orientation of the grains. The diffraction conditions select out only one set of grains, characterized by Miller indices (hkl) at a given scattering angle for a given wavelength. For example, if measurements are made with the {113} reflection in a particular sample orientation, only the average strain in the set of grains with <113> orientations in that direction is obtained. If measurements are made with the {002} reflection in the same sample orientation, only the average strain in the set of grains

with <002> orientations in that direction is obtained. The strains in the two sets of grains are different because of the different elastic responses to applied stress, i.e. different diffraction elastic constants, and because of intergranular strains if the component has yielded plastically.

Uniaxial loading experiments on 304L stainless steel [18,19], which is close in composition to 316 stainless steel, have shown how the intergranular effects are manifested. In the region below the yield point, in the elastic regime, the strain response of the different reflections in the stress direction is linear with slope given by $1/E_{hkl}$. However, once plasticity occurs some reflections depart from this linear response. In particular, a measurement of the response in the loading direction with the aid of the {002} reflection indicates that the <002> grains accumulate additional elastic tensile strains over and above the strain corresponding to the applied stress, $\frac{\sigma_{applied}}{E_{hkl}}$. The <220> grains show additional compressive strains. On unloading, <002> grains display tensile residual strains whereas <220> grains display compressive residual strains. Other grain orientations, particularly the <111> and <113>, follow an identical linear response in both the elastic and plastic regions. These grain orientations exhibit residual elastic strains that are, to within the experimental accuracy, zero. Strains of this nature, which vary between different orientations of grains, are said to be intergranular. They compensate for the different plastic deformations undergone by various sets of grains and the corresponding residual stresses must balance over the ensemble of grain orientations. In the presence of a load, the stresses that correspond to the intergranular strains will also sum to zero. However the strain, as measured with the {002} reflection, will be biased by the intergranular effects if plasticity has been involved. If the stress field is then calculated from the {002} strain, an erroneous estimate is obtained. Because the {113} reflection is, to within the experimental error, free from intergranular effects, it may be taken to give a correct measure of the strains corresponding to the stress field. For this reason the {113} reflection was chosen to map the stress field in these experiments. Conversely, the {002} reflection can be a good indicator of the presence of plastic deformation. If the process that lead to the stress field involved only elastic deformation, the {002} strain measurements should reproduce exactly the same stresses as the {113} reflection with the use of the appropriate diffraction elastic constant. On the other hand, if plasticity has been involved, the {002} stresses will differ from the {113} stresses. The agreement between {002} and {113} stresses is therefore a sensitive indicator of plasticity.

2b: Contour method

The relatively new contour [9] method measures a full cross-sectional map of residual stresses. The part of interest is carefully cut in two causing the residual stresses normal to the cut plane to relax. The contours of each of the opposing surfaces created by the cut are then measured. The deviation of the surface contours from planarity is assumed to be caused by elastic relaxation of the residual stresses and is used to calculate the original residual stresses.

Based on Bueckner's superposition principle [20], the original residual stresses on the cut plane are calculated by elastically displacing the cut surface, taken as flat, into the opposite shape of the measured contour. This is accomplished using a 3D, elastic Finite Element (FE) model. Because the measured contour provides information about the normal displacements of the cut plane but not about transverse displacements, the cut surface in the FE model is displaced only in the normal direction. The transverse displacements are left unconstrained, which in a structural finite element code means that the shear stresses normal to the cut plane are enforced to be zero. Even when the residual shear stresses were non-zero, the correct results for the normal stresses can be obtained. Residual shear stresses normal to the cut plane will cause anti-symmetric deformations on the two opposing surfaces created by the cut, i.e., a low spot on one surface and a high spot on the other. So long as the two surface contours are averaged, the correct result for the residual normal stresses is returned [9]. The averaging of the two surfaces also removes errors that could be caused if the flat-cut assumption was in error. If the cut wanders from the assumed cut plane or if the part moves during cutting as stresses are relaxed, the contours on the two surfaces are affected anti-symmetrically and the errors go away on averaging.

3. Experiments

3.1. Sample Preparation

As described in the introduction, the LENS® samples are fabricated layer by layer on stainless steel support plates. The initial choice for measurements in the thin wall and pillar was to provide insight into the stress states of complex parts made up of thin and thick sections as well as provide comparisons between two- and three-dimensional effects in heat flow through areas and volumes. For the thin wall, each layer is a single bead deposition in thickness and the sample simply traverses back and forth through the laser focus to generate the shape. A simple serpentine raster is used to produce each cross section of the pillar. An additional complexity for the pillar is that the raster changes angle of attack by 105° for each layer, which is important for the accurate fabrication of complex parts [21]. What this means is that it take six layers of deposition before the laser tracks the deposition line of attack of the initial layer. As with any fast solidification or welding-type process, the microstructure in any local section of the sample contains a variation in length scales. The travel velocities are small compared to the kinetic limitations of growth, and solidification should follow the heat flow direction resulting in a variety of growth directions and crystal orientations.

To understand the effects of rastering on growth directions and if this impacts the residual stress in the LENS® parts, three rectangular 316 stainless steel samples were chosen such that the directions of raster can be maintained along the length (0^o) only direction (similar to the thin wall plate [8]), along the short or thickness direction (90^o) and also use the rastering technique, called ISO as mentioned above where the angle of attack changes by 105^o deg for each added layer. In addition, the rectangular cross-section lies in-between the thin wall and pillar (square cross-section) geometry used in the previous study [8] and provides a comprehensive assortment of parts shapes which

would involve thin and thick sections typically found in prototypical structural components.
The 316 stainless steel pillar sample with a square cross-section was rastered using the ISO technique for studying the effect of plasticity using neutron diffraction. This was the same sample used in the previous study [8] where residual stress measurements were made using neutron diffraction. For the contour method, the 316 stainless steel and Inconel 718 samples with a square cross-section were rastered using the ISO technique.

3.2. Neutron Diffraction Experiments

3.2.1. Rectangular Plate (25x5x100mm^3) with various rasters.

The experiments were carried out on the L3 diffractometer in the neutron laboratory of the National Research Council, Canada at the NRU reactor, Chalk River, Canada. The details of the experimental set up and the configuration of the spectrometer for the neutron diffraction measurements are detailed elsewhere [8]. Neutrons of wavelength 1.5261Å were diffracted from the (115) planes of a germanium monochromator at a scattering angle of 89º. The intersection of the incident and diffracted beams were chosen to obtain a gauge volume of dimensions 1x1x2 mm^3 over which the strain is averaged. The {113} diffraction peak positions were determined by fitting Gaussian line shapes on a flat background to the count versus angle data. The typical uncertainty in the fitted diffraction angle was ±0.005° giving a precision in strain of ±0.5x10^{-4} and an upper bound in errors in stress determination within ± 30 MPa. The widths of the diffraction peaks were about 0.5^o.

A sketch of the rectangular plate is shown in Fig. 1 together with coordinate axes adopted to define directions. The schematic of laser rastering methods for fabrication the three rectangular samples and terminology used to identify them are shown in Fig. 2. The three samples with the supporting plates removed were mounted on an XYZ translator table under computer control so that any location in the wall may be brought into the gauge volume as shown in Fig. 3.

3.2.2. Pillar (13.5x13.5x45 mm^3)
A sketch of the pillar on its support plate and the coordinate axis system adopted to define directions as well as the loci of measurement are shown in Fig. 4. For the pillar the gauge volume was defined by 2mm wide slits in the incident and diffracted beams so the strains were averaged over a 2x2x2 mm^3 volume. To explore the effects of plasticity on residual stresses, three components of strain corresponding to {113} and {002} diffracting planes, parallel to X, Y and Z were measured as a function of axial position, Z, along the centerline of the pillar as shown in Fig. 4. Strains were also measured over the cross section of the pillar midway between the free end and the support plate higher spatial resolution using 1mm wide slits to explore the rapid change in stress state near the surfaces of the pillar.

3.3. Contour Method

3.3.1.

All of the specimens were cut using Wire Electric Discharge Machining (WEDM) under similar conditions. WEDM has proven to be ideal for contour-method cutting because it makes a very straight cut, does not remove additional material from previously cut surfaces, and does not induce plastic deformation like conventional contact-based machining does. WEDM has been extensively studied for applications to residual stress measurement, and it has been shown to result in negligible induced stresses if cutting is performed under the proper conditions [22]. For the specimens in this study, a Mitsubishi SX-10 wire EDM machine was used with a 100-μm diameter brass wire. The part was submerged in temperature-controlled deionized water throughout the cutting process. "Skim cut" settings, which are normally used for better precision and a finer surface finish, were used because they also minimize any recast layer and cutting-induced stresses [22]. For the contour method, it is preferred to minimize the amount the cut deviates from the original cut plane. Therefore, a small fixture similar to previous fixtures [10] was built to clamp the specimens during the cutting. To prevent any thermal stresses, the specimens and the fixture were allowed to come to thermal equilibrium in the water tank before clamping. Each sample was about 100 mm long and was cut into two 50 mm long pieces. The bases were left attached during and after the cutting. The 316 stainless sample cut in 25 minutes and the Inconel 718 sample cut in 23 minutes.

The contours of the cut surfaces were measured by laser scanning [10]. After cutting the parts were unclamped from the fixtures. The surfaces were scanned using a confocal laser ranging probe with a spot 7 μm in diameter, and the nominal accuracy of the probe was ±0.2 μm. The surface was scanned by rastering the probe using orthogonal air-bearing translation stages. The motions of the laser scanner were confirmed to remain flat to sub-μm accuracy by measuring an optical flat. The specimens in this study were scanned using rows separated by 0.1 mm with data points within a row sampled every 0.015 mm. This scanning density gave tens of thousands of data points per sample and took only a couple hours for each sample. The samples had similarly shaped contours: a dome with the high spot in approximately the center of the surface. For the 316 stainless steel specimen, the peak-to-valley amplitude of the contour was about 12 μm, and it was about 18 μm for the Inconel 718 specimen.

As described in 2b, the stresses that were originally present on the plane of the cut were calculated numerically by elastically deforming the cut surface into the opposite shape of the contour that was measured on the same surface. This was accomplished using a 3-D elastic finite element (FE) model. A model was constructed of one half of each specimen—the condition after each had been cut in two. Using the commercial code ABAQUS, the model used reduced integration, quadratic shape-function (i.e., 20 node) brick elements. The elements were cubes approximately 1 mm on a side. The material behavior was isotropic linearly elastic. For the 316 stainless the values used, Young's Modulus of 196 GPa and Poisson's ratio of 0.294, were the bulk values consistent with the single crystal values used to interpret the neutron diffraction data. For the Inconel 718, nominal values of 205 GPa and 0.284 were used. For the stress calculation, the opposite of the measured surface contour was applied as displacement

boundary conditions in the normal direction on the surface corresponding to the cut. The normal stresses on the cut surface were then extracted from the FE model.

The spline-smoothing process used to convert the discrete surface contour data, i.e., the point clouds, into a form suitable for calculating the stresses with the FE model is described in detail elsewhere [10]. The point clouds from the opposing surfaces were flipped and aligned to each other. The planar component of each surface was removed by determining the best-fit plane and then subtracting it from the data. Each data set was interpolated onto a common grid, and then the two surfaces were averaged point-by-point. The data were smoothed by fitting to a surface defined by tensor product splines. The amount of smoothing was chosen to minimize uncertainty in the calculated stress map. Finally, the height coordinates of the smoothed surface were evaluated at the locations of the nodes in the finite element model, the signs were reversed, and the results were written into the FE input deck as displacement boundary conditions.

4. Results

4.1 Neutron Diffraction

4.1.1 Rectangular Plate

The three residual stress components (σ_x, σ_y, and σ_z) for the three rectangular plates with 0^o, 90^o and ISO rastering as a function of position along the growth (Z), width (Y) and thickness (X), directions are shown in Fig. 5(a,b,c), Fig.6(a,b,c) and Fig.7(a,b,c), respectively. Fig.5(a,b,c) shows the stress components (σ_x, σ_y, and σ_z) along the growth direction (Z locus, Fig. 1a) which also corresponds to the sample build direction using layer by layer rastering. Fig. 6(a,b,c) shows the stress components (σ_x, σ_y, and σ_z) along the Y locus (Fig. 1b) or the width direction. Fig. 7(a,b,c) shows the stress components (σ_x, σ_y, and σ_z) along the X locus (Fig. 1c) or the thickness direction.

4.1.1.1 Stresses along growth direction (Z locus)

The scans along the centerline of the rectangular plates samples in Fig. 5(a,b,c) shows that the stresses are uniaxial and directed along the growth direction. The stress profiles for the three plates rastered 0, 90 and ISO to the width (Y) direction are similar. The largest stresses are compressive and along the growth (Z) direction. The stresses along the width (Y) direction are also compressive but smaller. The stresses along the thickness (X) direction are within experimental uncertainty close to zero. The largest compressive stress occurs in the 0^o rastered sample with an average value of –366 MPa and the lowest stress occurs in the 90^o sample with an average value of –315 MPa. The ISO sample falls in between with an average value of –335 MPa. The measured 0.2% yield strength and the ultimate tensile strength of tensile test samples made from 316 stainless steel by the LENS® process are ~445 and ~770 MPa respectively, [1] so the residual stresses are a large fraction of the yield point. The stress (Z) in the growth direction decreases strongly as the free end is approached. Since the stress normal to a free surface must be zero this stress variation is expected. At the location 2.5mm from the free end, a biaxial state of stress is also observed but is now directed along the top edge of the wall in the Y-direction.

4.1.1.2 Stresses along the width direction (Y locus)

The stress profiles along the width direction for the three plates (0, 90 and ISO) are shown in Fig. 6 (a,b,c) and are also similar as observed in the growth direction. The stresses measured along a Y-locus are at approximately the mid-height, Fig. 1(b), is also uniaxial with the stress directed along the growth (Z) direction. However, there is a steep gradient of stress between the center, which is in compression, and the edges of the plates, which is in tension.

4.1.1.3 Stresses along the thickness direction (X locus)

The stress profiles along the thickness direction for the three plates (0, 90 and ISO) are shown in Fig. 7(a,b,c) and are also similar to the width (Y) directions and this is not surprising. However it is to be noted that the balancing tensile stresses are strongly evident along this direction than along the width direction (Y Locus). This is because along the width direction the strain measurements were not sampled all the way into the edge. The high balancing tensile stresses are present within 1 mm from any edge of the sample and along the width direction (Y Locus) the strain sampling was done with 2.5 mm remaining from the edge. However since our objective for these stress measurements was to understand whether the rastering directions under which the samples were grown into final shapes influenced the residual stresses significantly. Therefore comparing the core compressive stresses is sufficiently adequate to formulate a conclusion. The stress profiles within the LENS® rectangular plate samples, except for the magnitudes are identical to the neutron diffraction measurements in a thin wall plate and square pillar published in reference [8].

4.1.2 Square Pillar (13.5,13.5,45 mm^3) – Effect of Plasticity on Residual Stresses

Following the discussion in Section 2., and to check whether plasticity had occurred when the residual stress field was being formed, measurements of the three strain components were made as a function of axial position at the center of the pillar using the {002} reflection. The three components of stress were calculated from the strains with the (002) elastic constants given in Table 1. The stresses along the centerline derived from the {002} strains are also shown in Fig. 8 and are seen to be identical to within the experimental uncertainty to the stresses derived from the strains obtained using {113} reflection. Stresses along X and along Y calculated from {002} strains are also shown in Fig. 8. Away from the center of the pillar the stress derived from the {002} strain is systematically more tensile, but it is noted that the shift is small, typically less than two times the measurement uncertainty. Thus, there is no strong evidence over the central region of the pillar that these are different from the {113} stresses. From the discussion in Section 2., this indicates that the inhomogeneous deformation of the pillar was close to elastic in the region examined.

The apparent stress behavior beyond 35 mm from the free end, near the support plate, is complex. The microstructure of the material close to the support plate is known to be different to that of the bulk of the material because of the enhanced cooling in that region. Consequently the chemical composition may vary in this region and small changes in solute concentration may account for the apparent changes of strain. The microstructure tends to stabilize about 3 mm from the support plate and remains the

same up to the free end [23]. It is also likely that the support plate will constrain the pillar and affect the stress-state in this region.

4.2 Contour Method

Residual stress contours for a 316 stainless steel pillar sample are shown in Fig. 9a. The sample cross-section even though square was smaller (10.9x10.9 mm^2) than the square pillar (13.5x13.5mm^2) used for neutron diffraction. A different sample was measured because the sample used for neutron diffraction was later annealed to ensure that stresses did relax to zero (and indeed they did), and at the time of contour measurements the smaller samples was the closest sample available. The comparison of stresses (σ_z) along the growth direction between the contour method and neutron diffraction on these two samples are shown in Fig. 9b. Note the stresses are shown for both X and Y orientations of the samples. There is strong agreement between the contour method and neutron diffraction stresses. The spatial resolution and number of points available for the contour method also captures the exact shape of the stress profile. Even though the two material cross-sections are not the same the similarity of the stress profiles are not surprising and expected. However the slightly smaller values of the sample measured by the contour method could be attributed to the smaller cross-sectional area of the sample compared to that measured by neutron diffraction.

One significant advantage of the contour method is the ease with which it can be applied to other materials once the methodology is established. Fig. 10 shows an excellent example of applying contour techniques to Inconel 718, a material of interest to both aerospace and onshore drilling applications, for the pillar sample having a square cross-section (10.9x10.9 mm^2). The results are similar to that of stainless steel but the relative magnitudes are higher (x1.5).

5. Discussion

The results from neutron diffraction and contour methods are summarized below before addressing the possible reasons for causing the state of residual stresses within the LENS® processed samples.

1. The residual stresses were primarily uniaxial, along the growth (Z) direction for all the sample geometries (Thin Wall [8], Rectangular Plate and Square Pillar [8]) and materials tested. Compressive stresses were measured in the core balanced by tensile stresses at the surface.
2. The core region of pillar sample showed no effects of plasticity as inferred by neutron diffraction measurements, however this does not prove whether near the surface or regions of tensile stresses are void of plastic effects. The maximum tensile or compressive stresses measured are within the tensile yield level stress for stainless steel (~445 MPa) and Inconel 718 (~ 1040 MPa).
3. The effect of laser rastering directions appears not to be a significant issue on the magnitude of residual stresses. The similar stress profiles shown for the rectangular plate reveal that there is some effect of rastering directions on residual stresses even though not significantly large enough to influence current processing methods.

4. The stress measurements on the rectangular plates samples were performed with the base support plates removed. The stresses in the rectangular plate measure similar in both magnitude and directions to that of the square pillar sample of approximately the same area in cross-section. Therefore the measurements on the rectangular plate samples rule out any possibility that the residual stresses are primarily due to the constraint effects from the base support plate on which they are built upon.
5. The similar stress profiles within 316 stainless steel and Inconel 718 suggest that the origin of stresses are thermal gradients and are independent of the materials used. Other reasons for stresses due to phase transformation (δ-ferrite to austenite – stainless steel) or the precipitation of second phase particles from solid solution as in an Inconel 718 superalloy if they exist are probably second order effects.

The puzzling, though experimentally unambiguous, aspect of the experimental results is that the stress-state is primarily along the growth or axial (Z) direction at distances beyond about 5mm from the free ends of the samples. A stress-state with compressive stresses within and tensile stresses at the boundaries of a component may occur if the edges are hotter than the interior. In this case, the shrinkage of the outside is constrained by the cooler interior. If the shrinkage is primarily along the length of the sample, then the stress on the edges will be tensile and directed along the growth direction. Due to the large coefficient of thermal expansion of 316 stainless steel, 15.9×10^{-6}, [24], the strains observed in the present experiments ($\approx 15 \times 10^{-4}$) can be generated by a relatively small temperature difference, $\Delta T = 15 \times 10^{-4} / 15.9 \times 10^{-6} \approx 100K$.

The temperature distributions in LENS® thin plate samples during the building process have been examined [6,25]. As the laser deposits material away from an edge, the pattern of heat flow is roughly circular in and near the melt pool as shown schematically in Fig. 11. However, at an edge, the heat flow is localized and the energy dissipates further into the previously deposited layers. Therefore, the edges of any geometry are much hotter during the initial solidification and cooling cycle than the interior section. It is plausible that a temperature distribution of this kind could lead to the axial character of the observed residual stresses especially since the process singles out the axial direction. In a similar way, the temperature gradients at the ends of the deposition rasters in the manufacture of the pillar could lead to the axial stresses at its edges. If this conjecture is correct, adjusting the process variables to maintain the same molten pool temperature at the center and edge of the part and reducing the dwell time of the laser at the end points of the raster should lead to reductions in the residual stresses [26]. Further reductions in the final stress state may be possible through auxiliary heating to control the bulk cooling gradients and final cooling cycle of the component [26]. These improvements may readily be tested by neutron diffraction.

Furthermore, if the above reasoning is correct than the process of having the edges hotter relative to the core during the cooling process is opposite to that of a conventional quenching process. Similar to a quenching process but opposite in sequence, the edges of the sample cool slower than the center, the thermal contraction of the hotter edges (relatively speaking) produce a strain mismatch between the edges and the cooler core of the sample which results in an initial distribution of stress which is tension

in the core and compressive at the edges. Since the hotter edges have a lower yield stress, it cannot support the compressive stress imposed at the edges and because of plastic deformation the edges shrink to relieve some of the stresses. When the edges finally cool down to ambient conditions, the total contraction will be greater for the edges than the center because the edge contracts owing to both cooling and plastic deformation. The edge will then be stressed in tension, and the center will be in compression. This also provides an explanation as to why the core regions did not see the effects of plasticity as inferred from neutron diffraction measurements. Besides this sheds some light as to why the holographic measurements indicated yield level residual stress at some locations of the materials tested, since the holographic measurements are surface measurements within a depth resolution of 0.5 mm [7].

When comparing the residual stresses for 316 stainless steel and Inconel 718 the following observations are made. The measured residual stresses within the Inconel 718 sample are ~1.5 times greater than 316 stainless steel. The maximum residual stresses in Inconel 718 are about ~0.45 times the tensile yield strength (~1100 MPa) and in 316 stainless steel about ~0.7 times the tensile yield strength (~450 MPa). Based on the discussion provided in the above paragraphs, the magnitude of residual stresses produced during the LENS® components build up process depends on the stress-strain relationships for these materials and the degree of strain mismatch producing during the cooling operation. For a given strain mismatch, the higher the modulus of elasticity (Young's modulus) of the metal alloy, the higher the residual stress. Further, since the residual stress cannot exceed the yield stress, the higher the yield stress, the higher the possible residual stresses. Therefore, the yield-stress-temperature curve for the metal alloy is also important. If the yield stress decreases rapidly with increasing temperature, then the strain mismatch will be small at high temperature because the metal can accommodate thermally produced volume changes by plastic flow. On the other hand, metals that have high yield strength at elevated temperatures, like superalloys (e.g. Inconel 718), will develop larger residual stresses. A comparison of the room temperature properties for Inconel 718 and 316 stainless steel shows that except for the tensile yields strengths (~1100 MPa for Inconel 718 and ~450 for 316 stainless steel), the modulus of elasticity, thermal expansion coefficients are similar [28,29]. Even the melting points are similar [28,29] suggesting it is not the temperature difference associated with the melting temperature of the respective materials.

To understand the possible magnitudes of the mismatch strains between the 316 stainless steel and Inconel 718 metal alloys, we examine the thermal diffusivity (thermal conductivity/density x specific heat) for the two metal alloys. It is well known that thermal diffusivity serves as a useful parameter in describing the strain mismatch during the quenching process. Low values of thermal diffusivity (D_t) lead to high strain gradients between the surface and the core regions and high values have the opposite effect. Referring to the thermal properties from the appropriate ASM handbooks [28,29] the thermal diffusivity (D_t) based on room temperature properties (are calculated to be 4.05×10^{-6} (m^2/s) for 316 stainless steel and 3.20×10^{-6} (m^2/s) for Inconel 718. What this means is that 316 stainless steel has a lower temperature mis-match gradient

compared to that of Inconel 718 between the surface and core regions. As a first approximation, the comparison between the thermal diffusivities (D_t) of 316 stainless steel and Inconel 718 explains why the residual stresses measured in Inconel 718 are higher than 316 stainless steel.

Furthermore, If we take the ratio of the thermal diffusivities between 316 stainless steel and Inconel 718 and assuming similar modulus of elasticity and thermal coefficient of expansion [28,29], this value should concur with the same ratio of the maximum stress measured in Inconel 718 and 316 stainless under these idealized conditions. On comparing the ratio's between the diffusivities and the maximum stress we get the values of 1.27 and 1.42, respectively. The differences shows that our idealized assumptions are simplistic to capture the complex thermal transients involved during the LENS® components build up and the cooling down process. However based on the simple and directional residual stress profiles measured by neutron diffraction and verified with contour method, this approach provides some guidelines for the ongoing and future modeling efforts. Besides the calculations are based on room temperature properties and the higher yield strengths at elevated temperatures for Inconel 718 compared to 316 stainless steel could explain why the residual stresses are even higher in Inconel 718 from calculations based on room temperature properties for both these materials. As discussed in the preceding paragraphs, because of the large coefficient of thermal expansions for these two materials, even a small temperature difference of 100 to 150^{o}K between the surface and core regions could generate the maximum stress values as measured in 316 stainless and Inconel 718, respectively. Therefore these temperature gradients could also be explained through the difference in thermal properties as given by the thermal diffusivity (D_t) parameters.

It is also interesting to recall that at distances of 2.5 and 5.0mm from the free end of the rectangular plate samples (Fig. 5 a,b,c) a uniaxial component of stresses directed along the top edge (Y-direction) is observed in the middle of the top edge. At the termination of the deposition and build process, the stress in the middle may thus resemble the stress expected for the "bead-on-plate " analogy. This observation was also made in the Thin Wall plate sample and are reported in reference [8]

If one likens the process of depositing the material to a series of bead-on-plate welds, one might expect that the stress would have been directed perpendicular to the growth direction [27]. Specifically, for the thin plate near the free end, one might have expected a stress directed along the top edge of the plate, tensile in the middle of the top edge but becoming zero near the sides [8]. Stress balance would be achieved by similarly directed compressive stresses below the top edge. For the pillar one might have expected a biaxial tensile stress state in the XY plane near the very top of the pillar, in the central region away from the edges, but balanced by a biaxial compressive stress state at greater depths. However, manifestly the stress axis is turned through 90° from that expected on the basis of the above argument and is directed along the axial direction with a maximum halfway up the height of the pillar. The residual stress that is observed in the bulk of the sample therefore does not originate in a bead-on-plate type

process but has more to do with the specific processing aspects of the deposition and cooling of the sample as a whole.

6. Conclusions

The residual stress distributions in two types of LENS® components having rectangular and square cross-sections, were mapped by neutron diffraction and the contour method. Over most of the volume of the components, the stress is uniaxial with compression at the center of the samples and tension at the edges and aligned along the growth direction. The magnitudes of the residual stresses were a large fraction (40-50%) of the nominal yield strength. Thermal transients during the build process are considered to be likely causes of the residual stress patterns but these have yet to be modeled to verify the conjectures.

7. Acknowledgements

We wish to acknowledge the assistance of John Fox at Chalk River in setting up the residual stress measurement experiments, and Mark Ensz and Daryl Reckaway for their help in manufacturing the LENS® samples. We also wish to acknowledge useful discussions with Professors William Hofmeister and Jack Beuth on solidification behavior and residual stress manifestation, respectively. Part of this work was supported by the U. S. Department of Energy under contract DE-AC04-94AL85000. Sandia is a multiprogram laboratory operated by Sandia Corporation, a Lockheed Martin Company, for the United States Department of Energy.

8. References

1. M. L. Griffith, D. M. Keicher, C. L. Atwood, J. A. Romero, J. E. Smugeresky, L. D. Harwell, D. L. Greene, Proceedings of the Solid Freeform Fabrication Symposium, August 12-14, Austin, TX, (Austin, TX: The University of Texas at Austin, 1996), p. 125, 1996.

2. C. L. Atwood, M. L. Griffith, L. D. Harwell, E. Schlienger, M. T. Ensz, J. E. Smugeresky, J. A. Romero, D. L. Greene, D. E. Reckaway, Proceedings of ICALEO '98, November 16-19, 1998, Orlando, FL, (Orlando, FL: Laser Institute of America) p. E-1 (1999).

3. M. L. Griffith, M. T. Ensz, J. D. Puskar, C. V. Robino, J. A. Brooks, J. A. Philliber, J. E. Smugeresky, W. H. Hofmeister, Mat. Res. Soc. Symp. Proc. 625, p9, 2000.

4. P. F. Jacobs, Rapid Prototyping and Manufacturing: Fundamentals of StereoLithography, The Society of Manufacturing Engineers, Dearborn, MI, 1992.

5. W. H. Hofmeister, M. L. Griffith, M. T. Ensz, J. E. Smugeresky, J. of Materials, 53, p30, 2001.

6. J. Beuth and N. Klingbeil, J. of Materials 53, p36, 2001..

7. M. L. Griffith, M. E. Schlienger, L. D. Harwell, M. S. Oliver, M. D. Baldwin, M. T. Ensz, J. E. Smugeresky, M. Essien, J. Brooks, C. V. Robino, W. H. Hofmeister, M. J. Wert, D. V. Nelson, J. of Materials Design 20, p107, 1999.

8. P. Rangaswamy, T.M. Holden, R.B. Rogge and M.L. Griffith, submitted to The Journal of Strain Analysis for Engineering Design, March 2003.

9. M. B. Prime, "Cross-Sectional Mapping of Residual Stresses by Measuring the Surface Contour After a Cut," Journal of Engineering Materials and Technology, 123, pp. 162-168, 2001.
10. M. B. Prime, R. J., Sebring, J. M. Edwards, D. J. Hughes, and P. J. Edwards, Experimental Mechanics, accepted March 2003.
11. Prime, M. B. and Martineau, R. L., Materials Science Forum, 404-407, p521-526, 2002.
12. M. B. Prime, M. A. Newborn, J. A. Balog, Materials Science Forum, p426-432, p435-440, 2003.
13. A.D. Krawitz and T.M. Holden, "The Measurement of Residual-Stresses using Neutron-Diffraction", MRS Bullettin; v.15, no.11, p.57-64, 1990.
14. E. Kröner, Z. Physik 5, 504, 1958.
15. M. E. Mangalick and N.F.Fiore, Trans. Metall. Soc. A.I.M.E. 242**,** p2363, 1968.
16. Handbook of Materials Science vol. 2 (edited by C.T. Lynch) CRC Press, 1975.
17. J. W. L. Pang, T. M. Holden, J.S. Wright and T. E. Mason, Acta mater. 48, p1131, 2000.
18. B. Clausen, T. Lorentzen, M.A.M. Bourke and M.R. Daymond, Mat. Sci. Eng. A259, p17, 1999.
19. T. M. Holden, R.A. Holt and C.N. Tomé, Material Science and Engineering, A282, p131, 2000.
20. Bueckner, H. F., Transactions of the American Society of Mechanical Engineers, 80, pp. 1225–1230, 1958.
21. M. T. Ensz, L. D Harwell, M. L. Griffith, Proceedings of the Solid Freeform Fabrication Symposium, August 10-12, Austin, TX, 1998, (Austin, TX: The University of Texas at Austin) p. 359, 1998.
22. Cheng, W., Finnie, I., Gremaud, M. and Prime, M. B., Journal of Engineering Materials and Technology, 116 (1), p1–7,1994.
23. W.H. Hofmeister, private communication.
24. ASM Metals Reference Book, 3rd edition, (edited by M. Bauccio) p.360 ASM Materials Park, Ohio, 1993.
25. W. H. Hofmeister, M. Wert, J. E. Smugeresky, J.A. Philliber, M. L. Griffith, and M. T. Ensz, J. of Materials 51 (In press) available from JOM-*e* online at www.tms.org/pubs/journals/JOM/9907/Hofmeister/Hofmeister-9907.html.
26. A. Vasinonta, J. L. Beuth, M. L. Griffith, A Process Map for Consistent Build Conditions in the Solid Freeform Fabrication of Thin-Walled Structures, Journal of Manufacturing Science and Engineering, Vol 123, November 2001, pp. 615-622
27. H. J.Stone, P. J. Withers, T. M. Holden, S. M. Roberts and R. C. Reed, Metal. Trans.A 30A, p1797, 1999.
28. ASM Metals Hand Book, Ninth edition, ASM Materials Park, Ohio, Volume 3, 1990.
29. ASM Metals Hand Book, Ninth edition, ASM Materials Park, Ohio, 1993, Volume 2, 1992.

TABLES

TABLE 1

Diffraction elastic constants for 316 stainless steel

hkl	E (GPa)	ν
111	242	0.23
002	152	0.33
220	211	0.265
113	184	0.294
E_{bulk} (Kroner)	196	0.282
E_{bulk} (316,experiment)[a]	193	

a.Ref [14]

TABLE 2

Specifications for the preparation of the samples

Specification	Rectangular Plate	Pillar
Layer thickness (mm)	0.508	0.508
Hatch spacing (mm)	0.508	0.508
Power (W)	390	438

Powder: 316 Stainless steel, -325 mesh or 45μm average diameter. (Stellite Coatings, Goshen, IN.) Typical powder flow rate 800gm/hr.

Figure Captions

1. Schematic of a LENS sample of rectangular cross-section showing the locations of neutron strains measurements and the co-ordinate system used for a) along growth direction (Z), b) along width direction (Y), and, c) along through thickness (X).

2. Schematic of the laser rasters used in creating the three LENS rectangular samples.

3. The three rectangular LENS samples with the supporting plates removed are shown mounted on an XYZ translator table under computer control on the L3 spectrometer so that any location within the sample may be brought into the gauge volume for strain measurements. The co-ordinate systems are also shown.

4. Schematic of the square LENS pillar samples with dimensions and co-ordinate systems used for stress measurements by neutron diffraction and contour techniques.

5. X, Y, Z components of stress in the three rectangular samples as function of position along the Z axis (or growth direction) along the centerline (X=0,Y=0) of each sample.

6. X, Y, Z components of stress in the three rectangular samples as function of position along the Y axis (or width direction) along the centerline (X=0,Y=0) of each sample.

7. X, Y, Z components of stress in the three rectangular samples as function of position along the X axis (or thickness direction) along the centerline (X=0,Y=0) of each sample.

8. X, Y, Z components of stress for the {113} and {002} hkl diffracting planes in the pillar (12.5x12.5x45 mm^3) sample as function of position along the Z axis (or growth direction) along the centerline (X=0,Y=0). The open symbols represent {113} hkl planes and the closed symbols are representative of {002} hkl planes.

9. A) A contour map of the Z component stress in an austenitic stainless steel pillar sample using the contour method. B) Comparison of the Z component stress between neutron diffraction and contour method along both X and Y locus direction on the cut-cross-section of the pillar samples.

10. Contour map of the Z component stress in inconel 718 pillar sample of dimensions 10.9x10.9x100 mm^3 using the contour method.

11. Schematic of the patterns of heat flow in a thin wall sample when the melt pool is (1) in the middle of the top edge and (2) when it is at the side edge of a thin wall plate (1x25.x100mm^3).

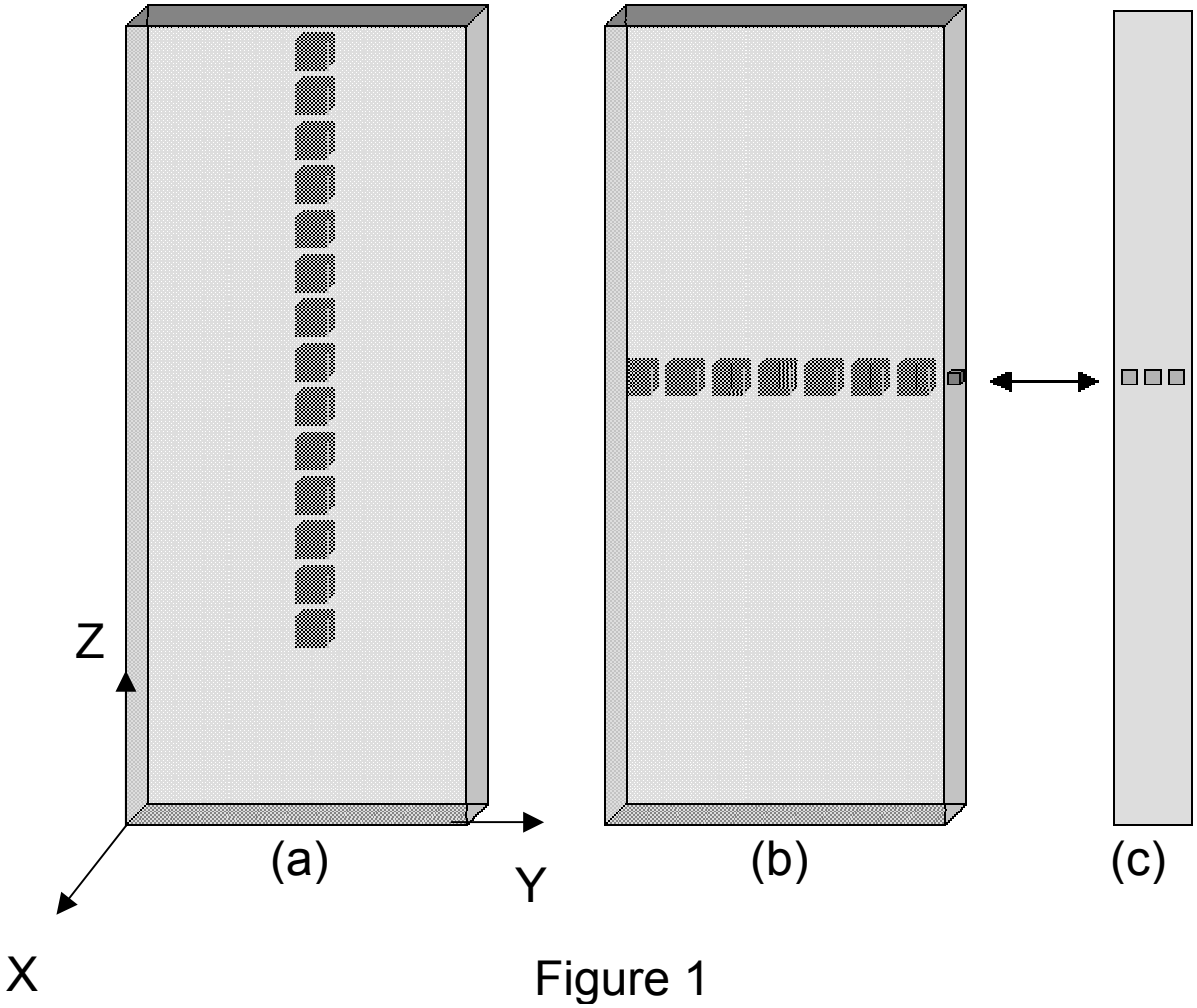

Figure 1

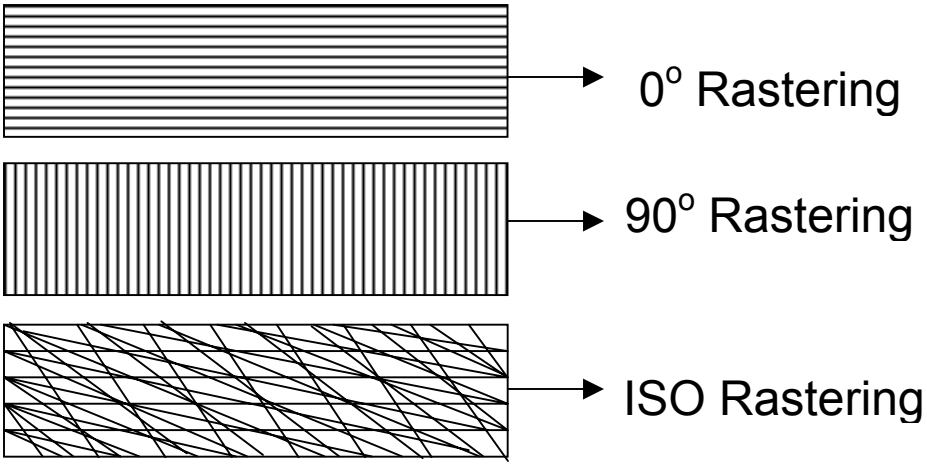

Figure 2

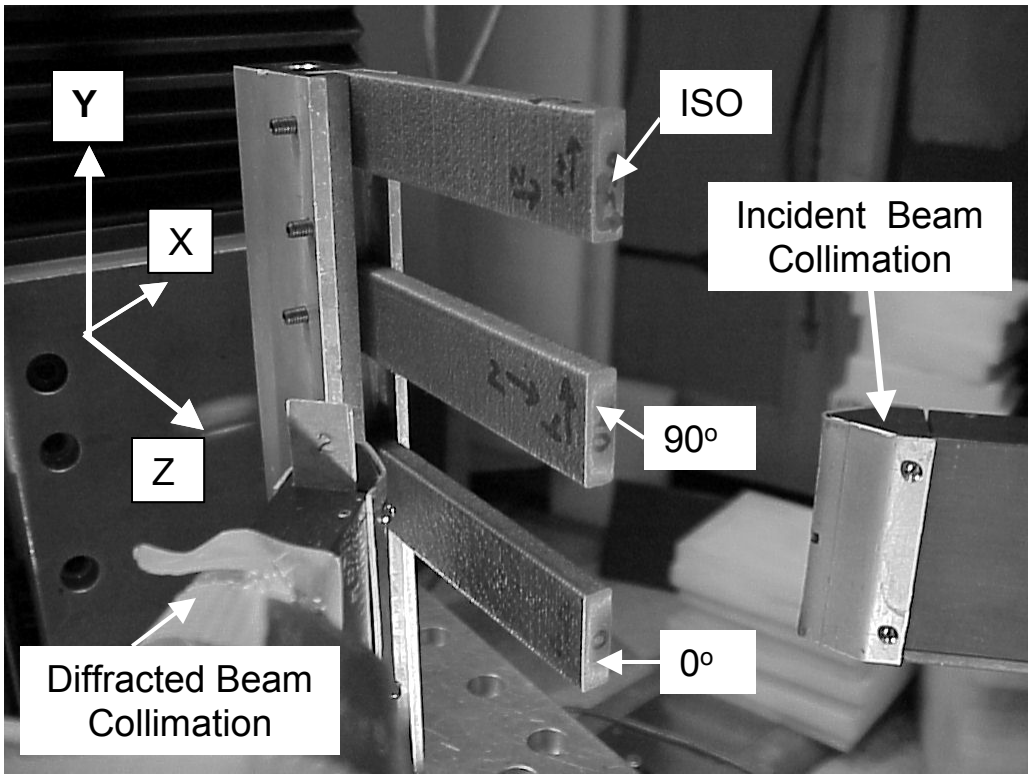

6 x 25 x 100 mm^3

Figure 3.

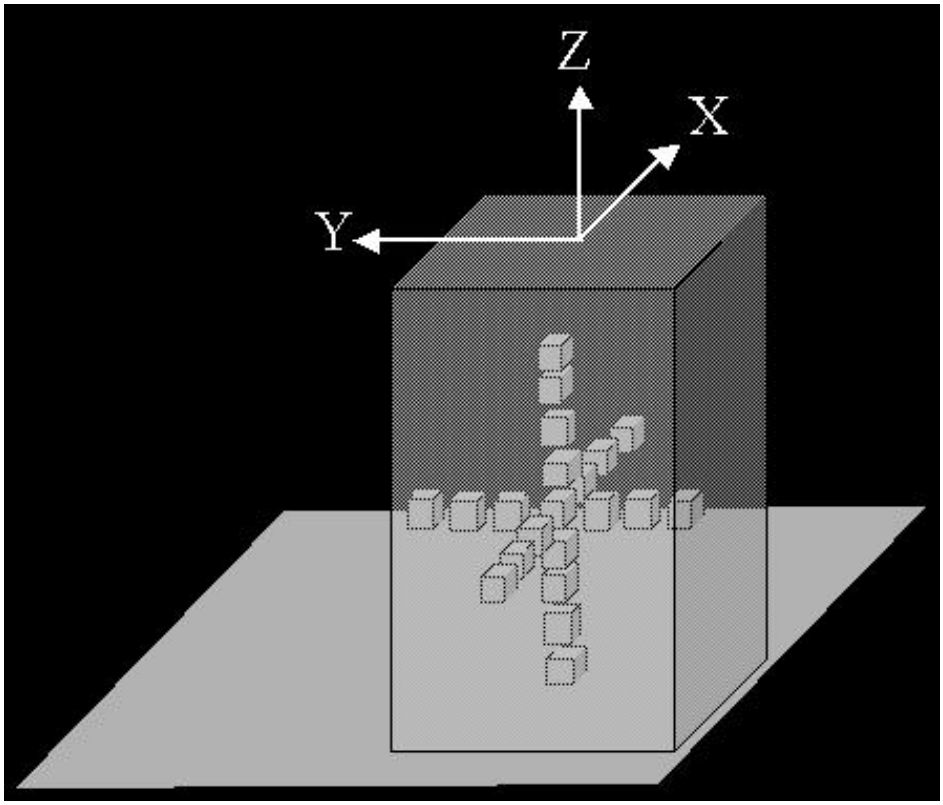

SQUARE PILLARS

(10.9 x 10.9 x 100 mm^3)
(13.5 x 13.5 x 50

Figure 4.

(a)

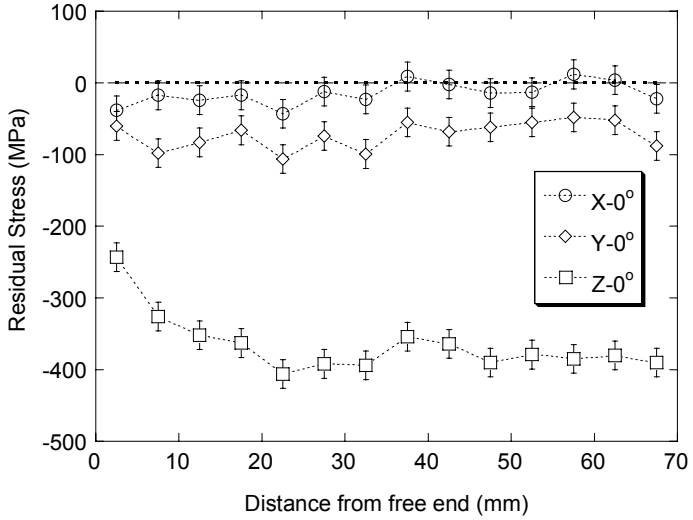
Residual Stress (MPa)
Distance from free end (mm)
X-0°
Y-0°
Z-0°

(b)

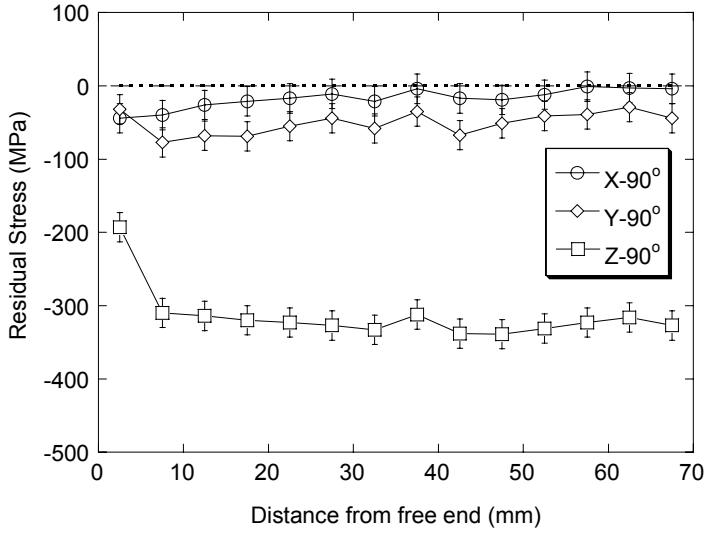
Residual Stress (MPa)
Distance from free end (mm)
X-90°
Y-90°
Z-90°

(c)

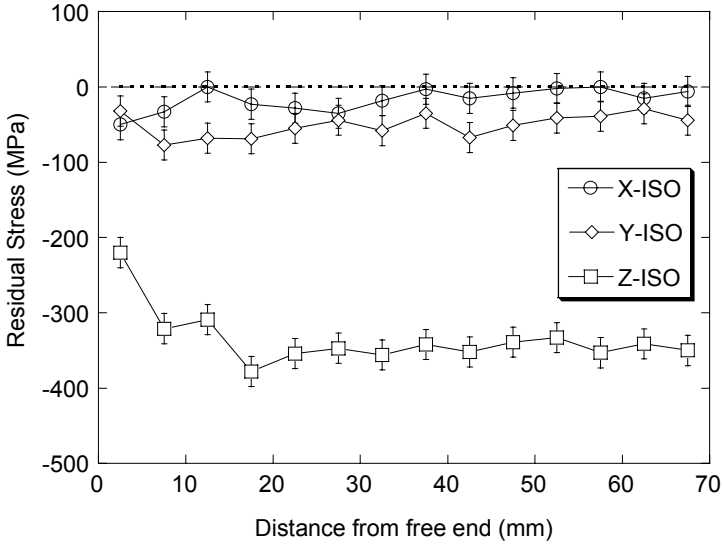
Residual Stress (MPa)
Distance from free end (mm)
X-ISO
Y-ISO
Z-ISO

Figure 5.

(a)

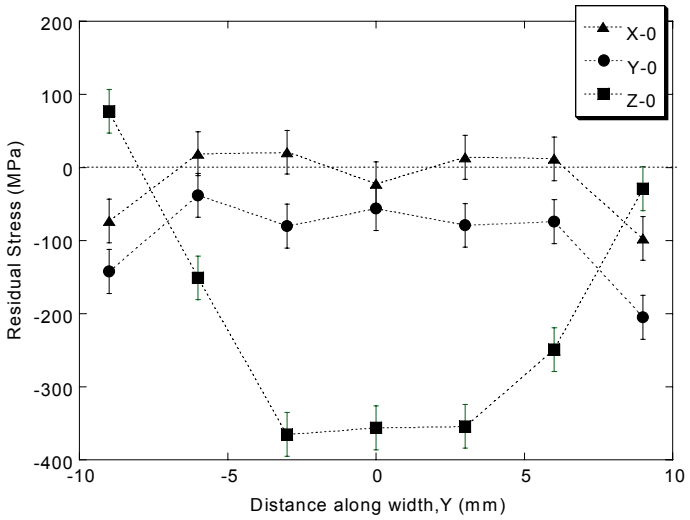
X-0
Y-0
Z-0
Residual Stress (MPa)
Distance along width,Y (mm)

(b)

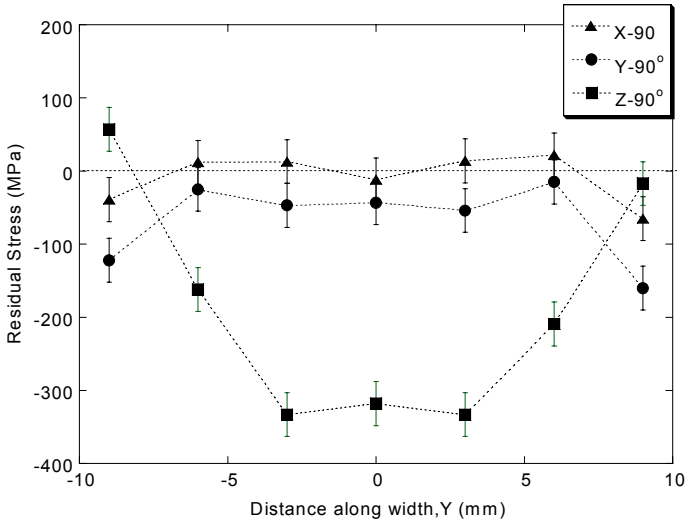
X-90
Y-90°
Z-90°
Residual Stress (MPa)
Distance along width,Y (mm)

(c)

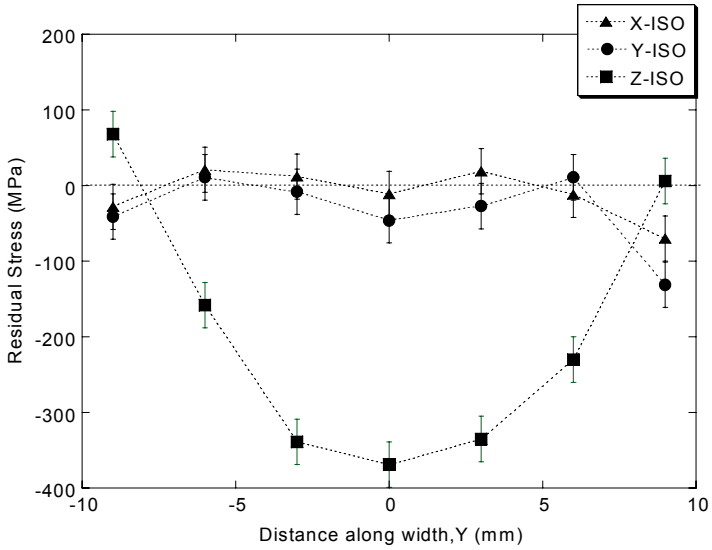
X-ISO
Y-ISO
Z-ISO
Residual Stress (MPa)
Distance along width,Y (mm)

Figure 6.

(a)

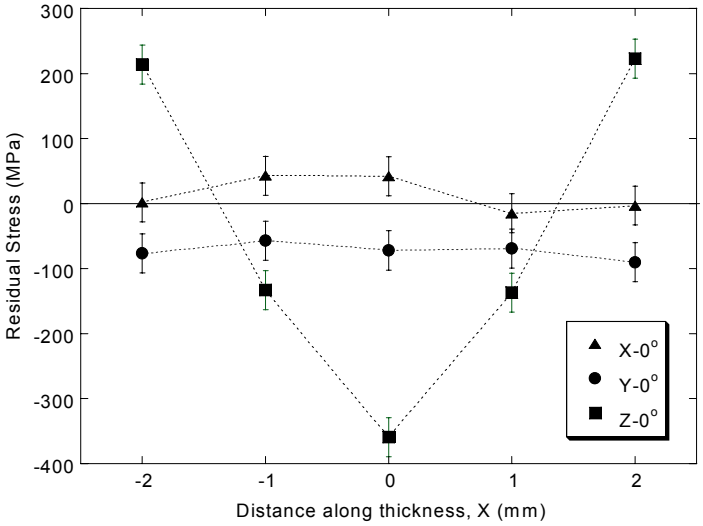
Residual Stress (MPa)
Distance along thickness, X (mm)
X-0°
Y-0°
Z-0°

(b)

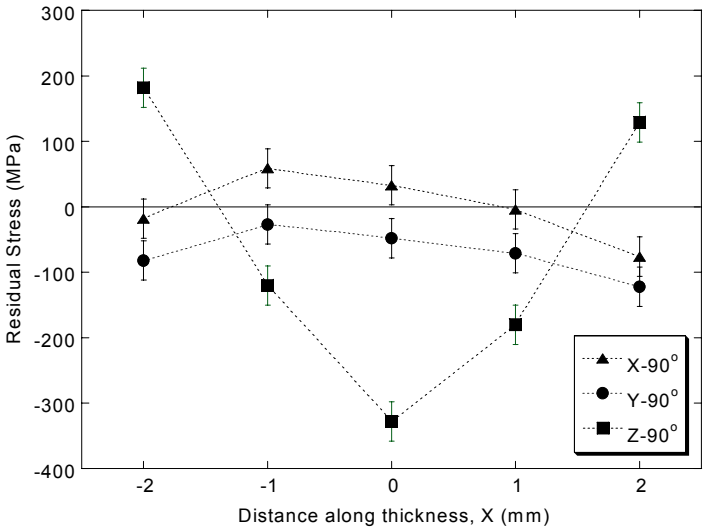
Residual Stress (MPa)
Distance along thickness, X (mm)
X-90°
Y-90°
Z-90°

(c)

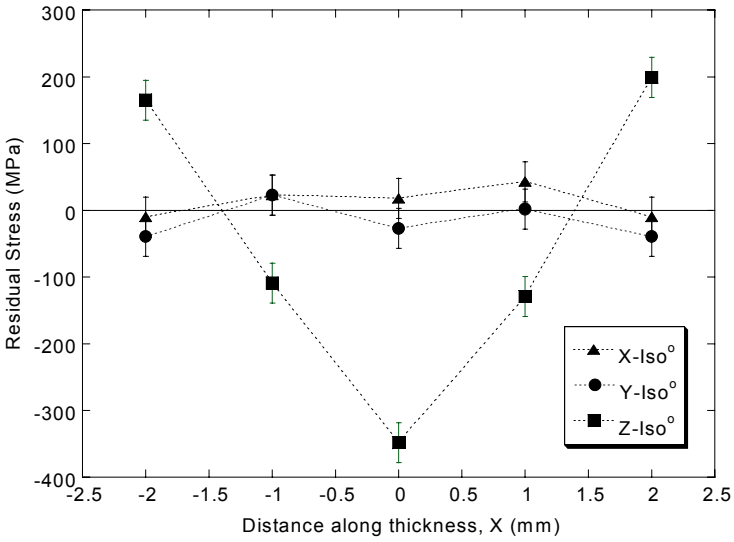
Residual Stress (MPa)
Distance along thickness, X (mm)
X-Iso°
Y-Iso°
Z-Iso°

Figure 7.

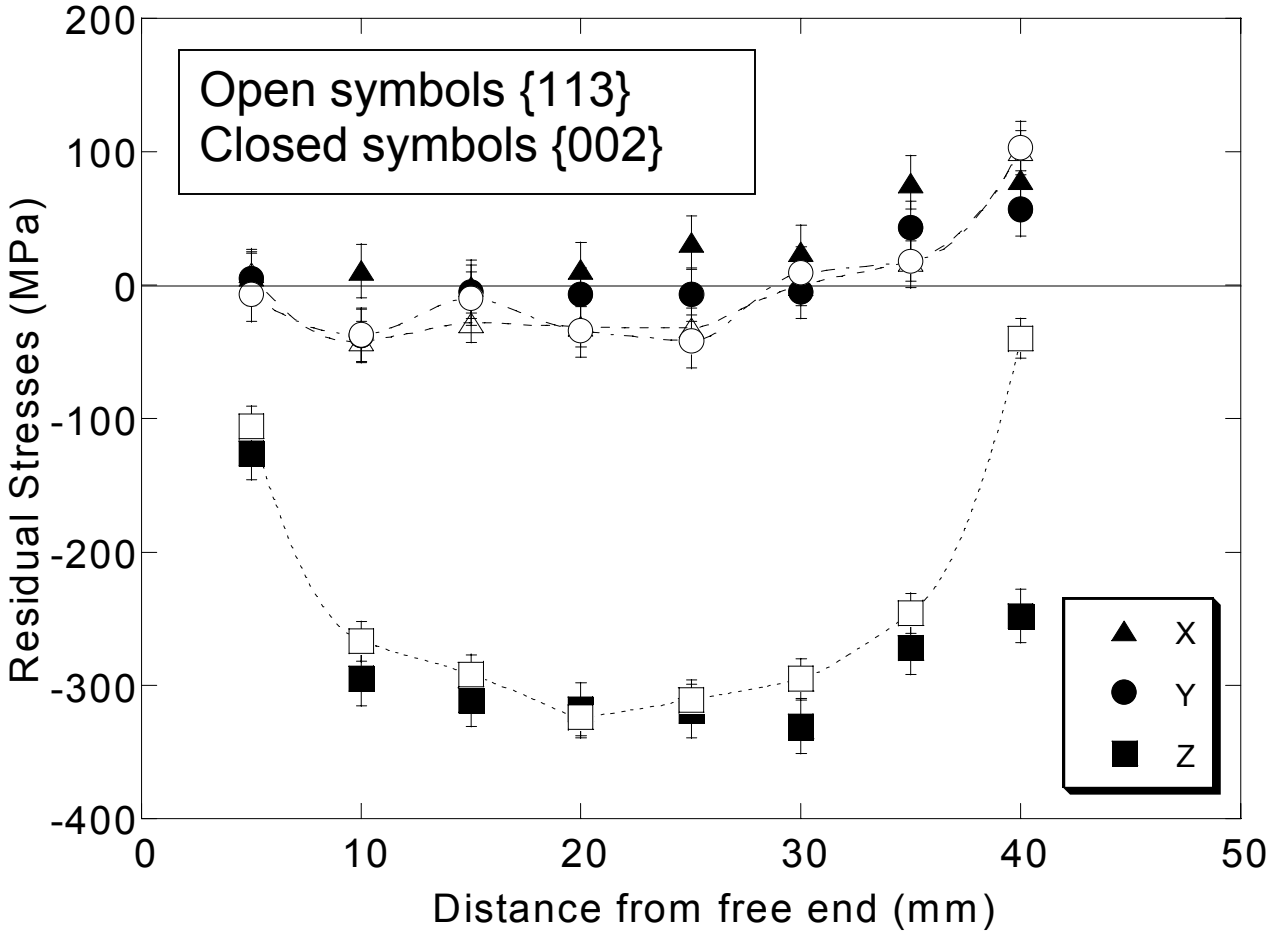
Open symbols {113}
Closed symbols {002}
Residual Stresses (MPa)
Distance from free end (mm)
X
Y
Z
200
100
0
-100
-200
-300
-400
0
10
20
30
40
50

Figure 8.

(a)

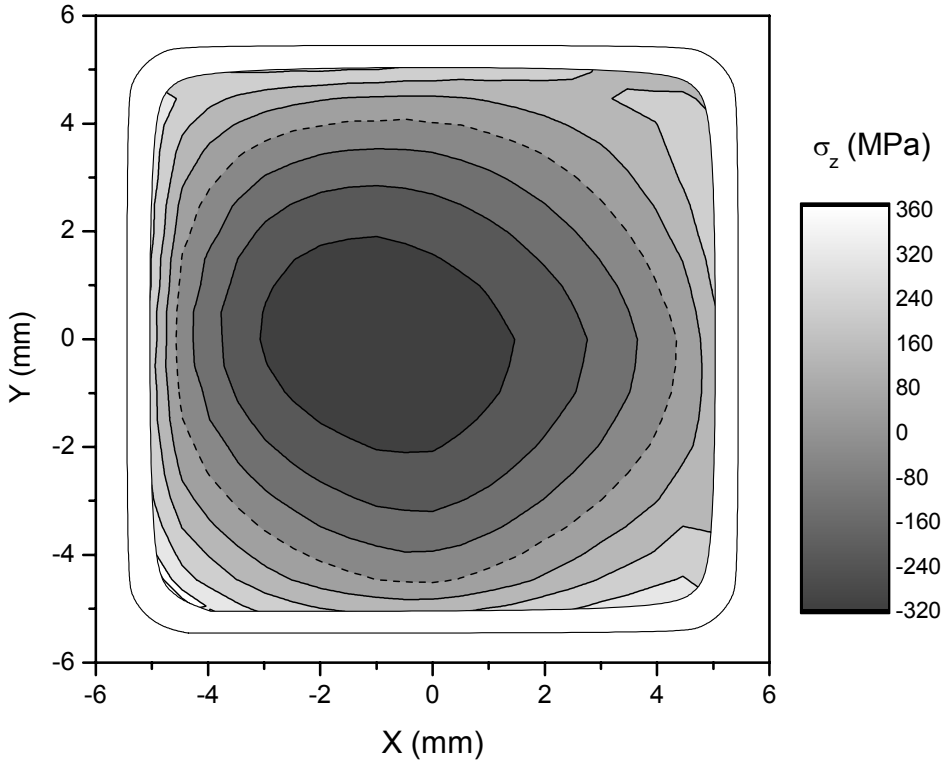
σz (MPa)
360
320
240
160
80
0
-80
-160
-240
-320
Y (mm)
X (mm)
6
4
2
0
-2
-4
-6

(b)

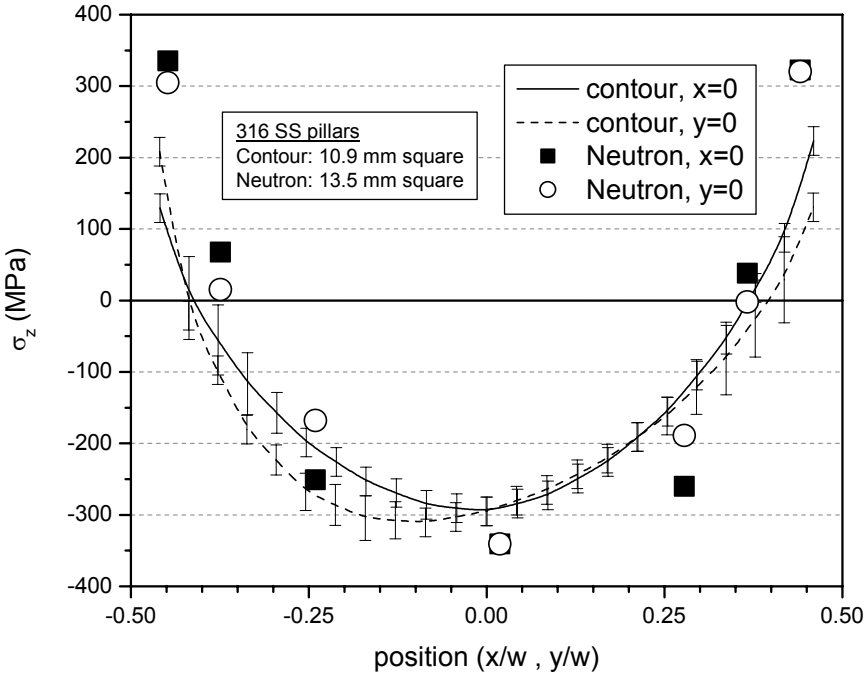
316 SS pillars
Contour: 10.9 mm square
Neutron: 13.5 mm square
contour, x=0
contour, y=0
Neutron, x=0
Neutron, y=0
σz (MPa)
position (x/w , y/w)
400
300
200
100
0
-100
-200
-300
-400
-0.50
-0.25
0.00
0.25
0.50

Figure 9.

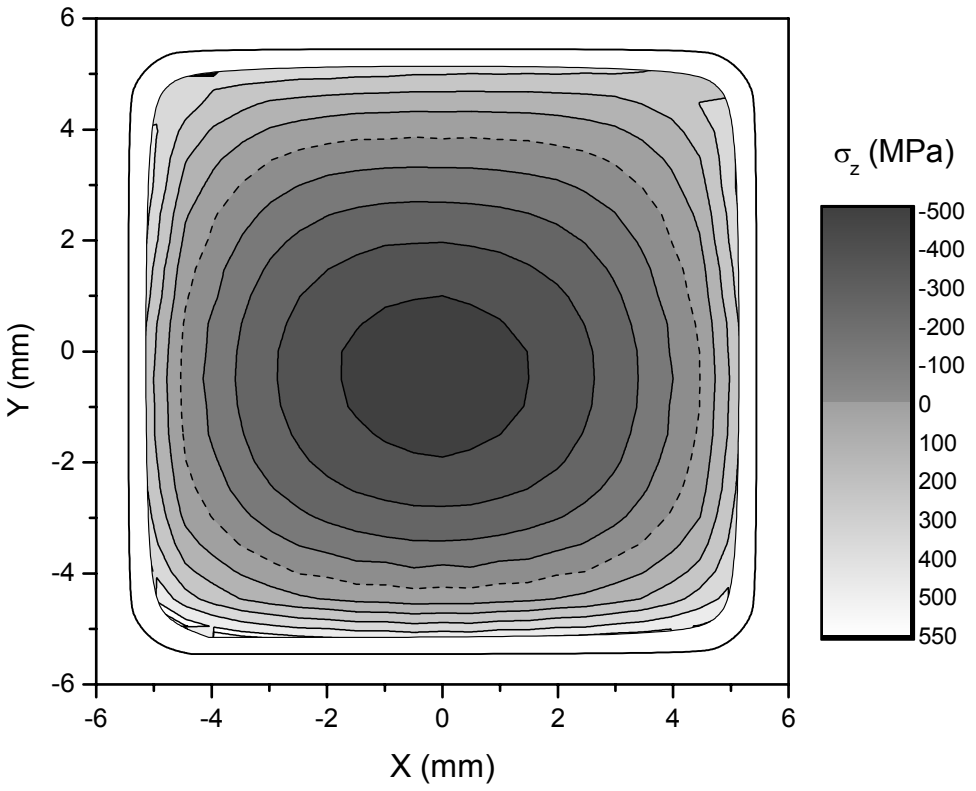

Figure 10.

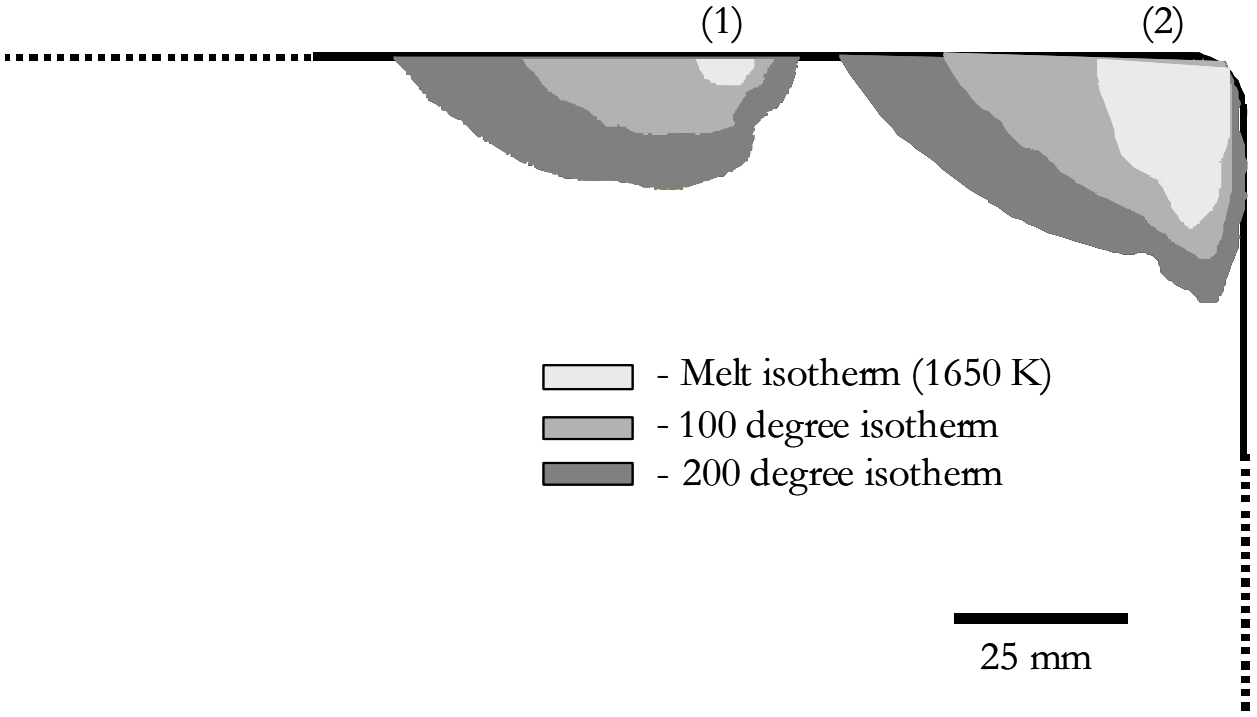

Figure 11.